Available online at www.sciencedirect.com

SciVerse ScienceDirect

Procedia Materials Science 1 (2012) 191 – 198

Procedia Materials Science

www.elsevier.com/locate/procedia

11th International Congress on Metallurgy & Materials SAM/CONAMET 2011.

Ab-initio studies on carburization of Fe_3Al based alloys

M. Forti [a, b, c, *], P. Alonso [b], P. Balbuena [c]

[a] *Instituto de Tecnología Prof. Jorge Sabato (UNSAM-CNEA), Argentina*
[b] *Comisión Nacional de Energía Atómica, Argentina*
[c] *Department of Chemical Engineering, Texas A&M University, TX, USA*

Abstract

Fe-Al based alloys exhibit excellent properties but suffer metal dusting in carburizing atmospheres. Surface composition can be a determinant factor in the solution of this problem. We calculate in this work the C adsorption energies in the $L2_1$ Fe_2AlX (X=Ti,V,Nb) structures and we study the influence of surface covering. Our results show the beneficial effect of Ti, suggesting that there could exist an activation energy to promote the incorporation of C in the subsurface layers when the surface is covered enough.

Keywords: $L2_1$ Fe_2AlX (X=Ti,V,Nb); adsorption energies; absorption energies; carburisation.

1. Introduction

During the last years, an increasing interest in Fe-Al alloys has arisen due to their outstanding corrosion resistance (Bai et al., 2009, Grabke, 1999), specific stiffness, good wear resistance (Itoi et al., 2010) and good processability (Froes and Suryanarayana, 1996). Depending on alloying elements, creep resistance can be as good as for some Ni based alloys (Palm et al., 2007), but with a composition that allows lower costs. Its use as a binary alloy can be extended up to 600ºC, due to the coexistence of the iron disordered phase with ordered Fe_3Al ($D0_3$) phase (Palm, 2009) that favors mechanical resistance.

Recently, several hardening mechanisms have been investigated in order to extend the applicability range of Fe-Al alloys. As Schneider showed out (Schneider and Sauthoff, 2004), coherent precipitation of $L2_1$

* Corresponding Author, Tel. : +541167727832,
E-mail address: morti@cnea.gov.ar

2211-8128 © 2012 Published by Elsevier Ltd. Selection and/or peer-review under responsibility of SAM/CONAMET 2011, Rosario, Argentina.
Open access under CC BY-NC-ND license. doi:10.1016/j.mspro.2012.06.026

ordered phases gives rise to an improvement of mechanical properties. This type of precipitation can be found in the Fe-Al-X system with X=Ti (Krein et al., 2010), V (Maebashi et al., 2004) and Nb (Prymak and Stein , 2010). $L2_1$ phase can be found in these systems for narrow composition ranges in the Fe_2AlX region. Ti and V containing precipitates are thermodynamically stable, while Nb forms a metastable compound. However, time for decomposition below 500ºC is long enough to take it into account. The compounds that exhibit coexistence between ordered $L2_1$ – disordered A2 reach the best compromise between maximum work temperatures and yield stress.

Despite their excellent corrosion resistance, Fe-Al based alloys experience the detrimental phenomenon of metal dusting as demonstrated by Bernst, 2006; and Strauß, 1996. This mechanism differs from other corrosion mechanisms since it is not due to an electrochemical reaction between the metal surface and the environment. As Grabke points out (Grabke, 2003), when the metallic surface is exposed to a high carbon potential atmosphere, it plays the role of catalyst of molecules such as CO_2, CO or CH_4; C atoms are afterwards adsorbed C atoms, and finally absorbed. Oversaturation of C favors the formation of carbides, but the subsequent absorption of C promotes the formation of graphite. Destabilization of carbides release carbon atoms that form graphite which is immediately able to grow inside the surface. Metallic atoms diffuse through graphite layers to segregate outside and to form microparticles with a high specific area that accelerates the dissociation of molecules containing carbon.

Together with the high research activity dealing with metal dusting problem, there exist a few reported works involving the influence of ordered precipitates on the metal dusting resistance of Fe-Al alloys. Schneider and Zhang, 2003 reported that C and Ti presence on Fe_3Al based alloy drastically reduces metal dusting susceptibility in rich CO atmospheres, while Nb and V presence induces a minor reduction of the problem. The authors find that a protective alumina layer can explain this behavior. Ramírez-Caballero et. al., 2009, performed first principles calculations to obtain a complete map of the stable C adsorption sites on Fe_3Al $L1_2$ surfaces. They also searched for the diffusion paths for C incorporation to the surface, and they find that the presence of more C atoms around the adsorption site drastically reduces the energy barrier for C incorporation.

The present work is based on the hypothesis that adsorption properties can be modified by surface composition. They can be playing a fundamental role in metal dusting susceptibility determination. We calculate the C adsorption energies in the Fe_2AlX (X=Ti,V,Nb) $L2_1$ structures. In this frame, we study the influence of surface covering.

2. Calculation details and methods.

We use the Density Functional Theory (Hohenberg and Kohn, 1964) (DFT) implemented in the Viena Ab Initio Simulation Package (VASP) (Hafner, 2007), that is based on the expansion of wave functions in plane waves. The ion-electron interactions are treated using augmented projected waves (PAW)(Vanderbilt, 1990). The plane wave expansion is used with a cutoff energy of 400 eV. The exchange and correlation interactions are treated within the generalized gradient approximation (GGA) as described by Perdew et al., 1996. Integrations in the Brillouin zone are performed in a Monkhorst-Pack grid (Pack and Monkhorst, 1977) with a size of 4×4×4 for bulk models and of 4×4×1 for surfaces, and a Methfessel-Paxton parameter (Methfessel and Paxton, 1989) of 0.2 eV for the smoothening of occupation functions.

$L2_1$ cell can be understood as a cubic structure where vertexes of the cube are occupied with Fe atoms and Al and X atoms alternate in the center of the faces, as it is shown in Figure 1**.** The lattice parameter of the bulk in each compound is obtained by fitting total energy as a function of volume to a Birch-Murnaghan (Birch, 1947) equation of state. Results agree with literature, as it can be seen in Table 1.

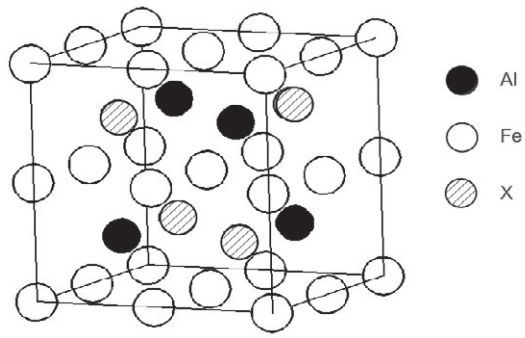

Figure 1: $L2_1$ structure for Fe_2AlX compounds.

Table 1: Lattice parameters for $L2_1$ structures. [c]Experimental Ref.,[*] Ab Initio Calculations.

X	Lattice parameter (Å)	
	This work	Literature
Fe	2.87	2.89 [c](Taylor and Jones, 1958) 2.76 [*](Lechermann et al., 2002)
Nb	2.96	2.91 [c](Morris et al., 2005)
Ti	2.91	-
V	2.85	2.88[c](Nishino et al., 1997) 2.85 [*](Kumar et al., 2009)

2.1. Adsorption

The model for Fe_2AlX intermetallic surfaces was constructed from the stacking of four atomic layers with (1 1 0) orientation in a ABAB sequence leading to 64 atoms super cells. The (110) plane was chosen as the most dense plane in the $L2_1$ structure. A 12 Å thick vacuum was allocated over the last atomic layer in order that the interaction between surface and its subsequent images could be neglected. Atomic positions on the (110) plane are sketched in Figure 2 together with the chosen supercell. In this way eight geometrically different positions are available for analysis through adsorption studies. Besides, 64 supercell sites are available for coverage studies. The strategy consists in covering the surface with an increasing number of carbon atoms allocated at the adsorption sites initially studied. The two lower layers are kept fixed in the bulk geometry while the carbon atoms are free to relax from an initial position at aprox. 1 Å above the surface. Adsorption energy E_{ads} is calculated for the different possible structures as a function of the number of adsorbed carbon atoms N, equilibrium total system energy E_{slab-C}, clean surface energy E_{slab} , and isolated carbon atom energy:

$$E_{ads} = \frac{1}{N}\left(E_{slab\text{-}C} - (E_{slab} + N a E_C)\right) \quad (1)$$

In the case where only one carbon is on the surface, we analyzed the eight positions shown in Figure 2**.** Three atom coverage was studied in several combinations of these eight sites. Then, we calculated adsorption energy for coverages of 0.25, 0.375, and 0.5 ML / cell (16, 24, and 32 carbon atoms / cell), related to the 64 available sites. For 0.25 ML, we considered atoms only at sites *top* (16-A) or only at sites *hollow* (16-B). For 0.375 ML carbon atoms were placed at sites *top Fe* (24-A) or *on X* and *top Al* (24-B).

2.2. Absorption

Absorption studies were performed with six layer $L2_1$ surfaces constructed by AB-AB stacked (1 1 0) planes, with a 12 Å thick vacuum above the surface. The lower two layers were fixed to the bulk geometry. While only octahedral sites were analyzed as possible absorption sites, several cases were identified taking into account the relative octahedron orientation and its composition (Figure 3): octahedron with its axis perpendicular to the surface (*v sites*), or with one face parallel and as part of the surface (*h sites*). Three cases were considered for both v and h sites in accordance with the atom on the surface: a for Al, b for X, and no indication for Fe. For each of the six octahedral several initial positions were evaluated and it was verified that the geometrical centre was the equilibrium position. The same analysis was performed for the octahedron placed immediately below the surface (*level 1*) and for the subsequent below it (*level 2*). It was verified that the adsorption energy values were not meaningfully modified when calculated for this six layer model.

Absorption energy $\boldsymbol{E}_{\mathrm{abs}}$ is calculated as:

$$\mathrm{E_{abs}}=\frac{1}{\mathrm{N}}\left(\mathrm{E_{C\text{-}abs}}\text{-}(\mathrm{E_{slab}}+\mathrm{N}\times\mathrm{E_C})\right) \tag{2}$$

where $\boldsymbol{E}_{\boldsymbol{C}-\mathrm{abs}}$ is the absorption system energy, $\boldsymbol{E}_{\boldsymbol{slab}}$ the free surface energy, $\boldsymbol{N}$ and $\boldsymbol{E}_{\boldsymbol{C}}$ the number of carbons and the isolated carbon atom energy respectively.

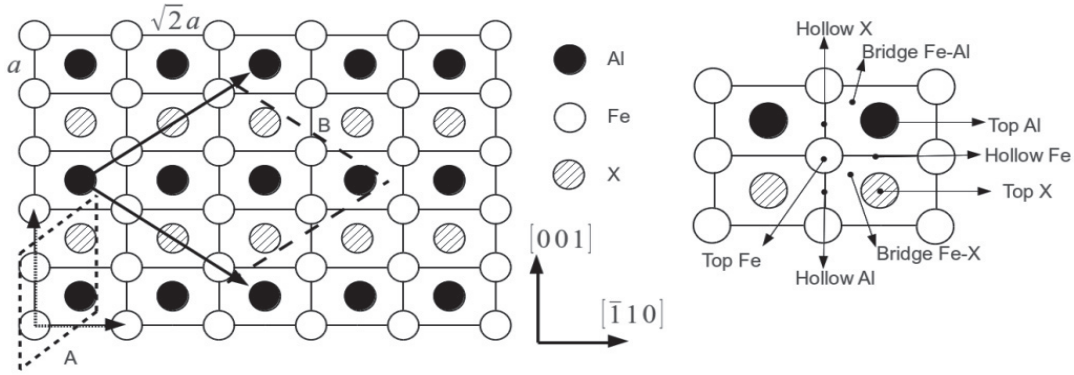

Figure 2**:** Left: (110) plane in $L2_1$ structure, where the lattice vectors are shown. Unit cell of the bidimensional structure (A) and chosen unit cell of the supercell (B) are shown. Right: adsorption sites.

3. Results

3.1. Adsorption

The absolute value of adsorption energy is higher for *hollow* sites tan for the others, and they can then be considered as equilibrium positions. Figure 4 shows the adsorption energy values for the *hollow* sites within the three systems in this work. Besides, it was also observed that while carbon atoms do not migrate to other sites when they are free to relax from their initial positions, the bridge sites migrate till they find an equilibrium position at the nearer *hollow* site. Table 2 shows distances between the adsorbed carbon and the surface at equilibrium, measured as the average value among the heights differences between carbon atom and the four atoms at the surface around the site. *hollow Al* sites are the furthest from the surface, while the carbon atom at the *hollow Fe site* is placed nearly at the same plane of the surface. Curiously, it is observed that adsorption is more intensive at *hollow Al* sites. This trend evidences carbon affinity with atoms around hollow

Al sites. The *hollow Fe sites* become unstable by the presence of Al in one vertex of the hollow site, leading to distortions when a carbon atom is inserted in the surface plane (Table 2).Adsorption energies for uniform coverages less than 0.25 ML exhibit almost the same values than one atom adsorption energies. In these cases there is no interaction between carbon atoms. However, trimmer formation was analyzed by combining three nearest sites. Stable trimers were found in sets of *hollow* sites joined by a *bridge* site as *hollow Fe – bridge Fe X – hollow Al*. Curiously, adsorption energies per carbon atom are similar in all cases and approximately equal to - 8.8 eV. For coverages of 0.25 and 0.375 ML, the system relaxes forming combinations of dimers and trimers with adsorption energies that approximately equal 7.3 eV, (Table 3). For 0.5 ML the equilibrium configuration is a distorted graphene layer.

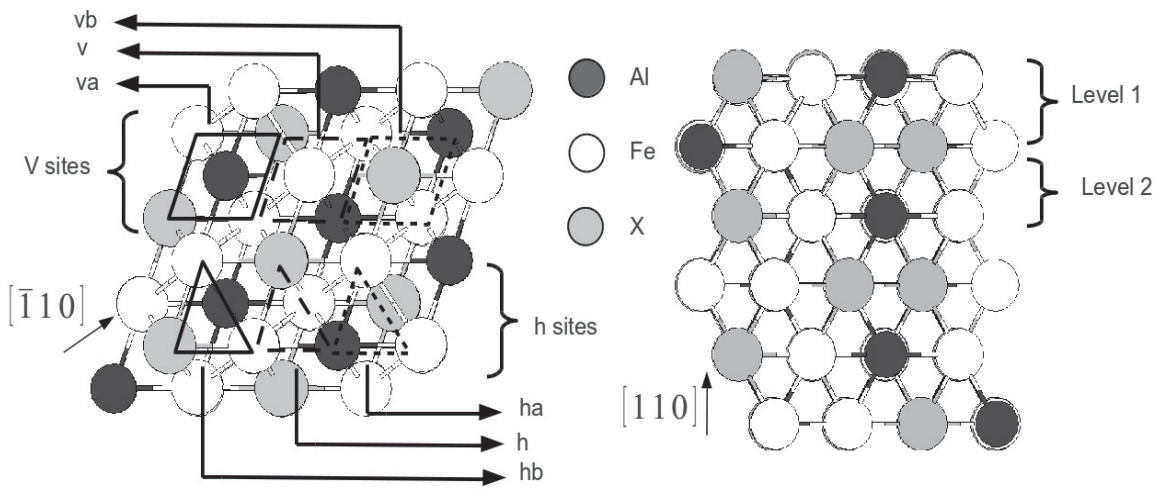

Figure 3**:** Octahedral sites used for absorption studies on the $L2_1$ surface.

Table 2**:** Distortion in *hollow* sites, as a percentage. Rows named S: surface distortion; remaining rows: distances between atoms in opposite verteces.

%		X		
		Nb	Ti	V
Hollow Al	S	-0.07	4.12	0.08
	Fe-Fe	-3.2	0.9	-1.0
	X-X	3.3	3.2	1.1
Hollow Fe	S	20.3	21.3	23.4
	Fe-Fe	-9.2	-9.6	-7.6
	Al-X	32.4	34.2	33.6
Hollow X	S	2.0	5.1	3.4
	Fe-Fe	4.0	7.8	4.2
	Al-Al	-1.9	-2.5	-0.8

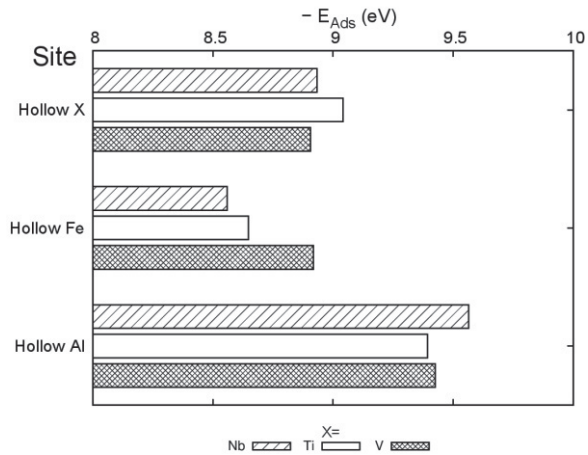

Figure 4: Adsorption energies for Hollow sites.

3.2. Absorption

For each octahedron, the C atom is in equilibrium at the geometric center. Figure 5 shows a comparison between absorption energies for each case and the change in energy between levels 1 and 2. The most intensive absorption energies are found for X=Ti. Furthermore, for X=Nb and X=Ti the intensity of absorption energy decreases on going from level 1 to level 2, while for X=Ti energy difference between both levels is almost negligible on sites *v*.

These calculations become relevant when absorption energies are compared with adsorption ones, as it is shown in Figure 6. For large coverages and for X=V, Nb adsorption sites are energetically favored face to absorption sites. On the other hand, for X=Ti, the strong bond of absorption states reverses the mentioned trend and favors the absorption states. Therefore in this case, driving forces could exist capable to promote C incorporation to the subsurface levels when the surface is sufficiently covered.

However, in order to conclude that these Ti alloys are more resistant to Metal Dusting, it is necessary to have a deep insight into diffusion paths and migration energies for C atom towards the subsurface levels, and its dependence with surface coverage.

Table 3: Adsorption energies (eV) per adsorbed atom as a function of coverage

ML	Initial condition	X		
		Nb	Ti	V
0.25	16A	-4.23	-7.01	-7.26
	16B	-7.37	-7.2	-7.22
0.375	24A	-7.11	-7.38	-7.26
	24B	-7.04	-7.14	-7.1
0.5	32A	-7.61	-7.54	-7.63

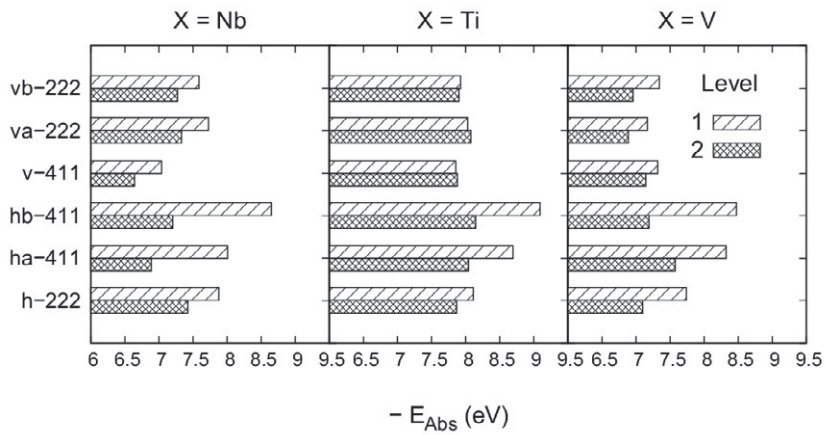

Figure 5: Absorption energies for all systems.

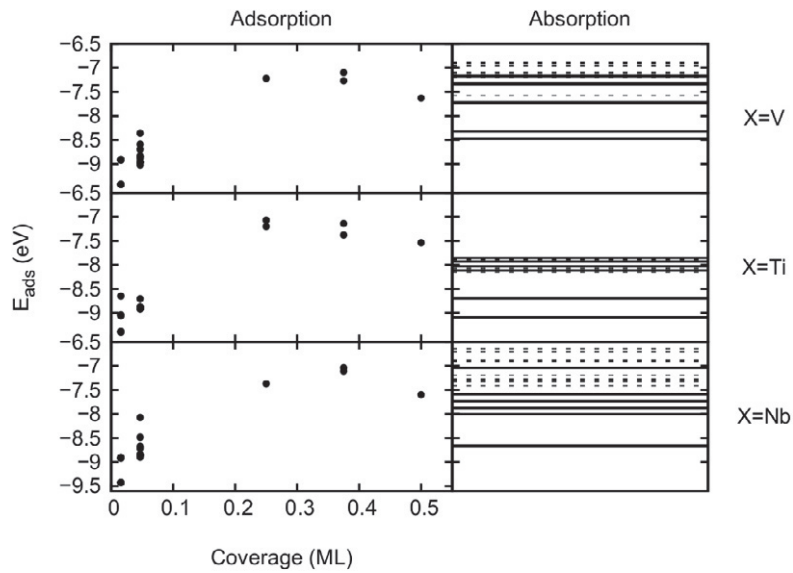

Figure 6: Comparison between adsorption and absorption results

4. Conclusions

The findings in this work are relevant as they show that the intrinsic surface characteristics could have a non negligible influence on their resistance. We show trends for carbon atoms adsorption and absorption on L21 Fe2AlX (X=Ti,V,Nb) surfaces, and suggest that the resulting relatively high intensity absorption energies for X=Ti could be related with a better resistance to metal dusting of titanium alloys. To have a deeper insight in this area, future work should be focused on diffusion paths and activation energies.

Acknowledgements

Financial support from the Department of Energy, Basic Energy Sciences, grant DE-FG02-06ER15836 is gratefully acknowledged. This research used resources of the TAMU Supercomputer Center and from Texas A&M University Brazos HPC cluster.

References

Bai, Q., Wang, X. Fan, W., 2009. Study on Seawater Corrosion of Fe-Al Intermetallic Compound, Advanced Materials Research 79-82, p. 1915.

Bernst, R., Schneider, A., Spiegel, M., 2006. Metal dusting of binary iron aluminum alloys at 600 °C. Materials and Corrosion 57, p. 724.

Birch F., 1947. Finite Elastic Strain of Cubic Crystals. Physical Review 71, p. 809.

Froes, F., Suryanarayana, C., 1996. Iron Aluminides, in "*Physical Metallurgy and Processing Of Intermetallic Compounds*" Stoloff, N., Sikka, V. editors. Chapman & Hall, New York.

Grabke, H., 1999. Oxidation of NiAl and FeAl. Intermetalics 7, p. 1153.

Grabke H.J., 2003. Metal dusting. Materials and Corrosion 54, p. 736

Hafner J., 2007. Materials simulations using VASP—a quantum perspective to materials science. Computer Physics Communications 177, p. 6.

Hohenberg P., Kohn W. 1964. Inhomogeneous electron gas. Physical Review 136, p. B864; Kohn W., Sham L.J., 1965. Self-Consistent Equations Including Exchange and Correlation Effects. Physical Review 140, p. A1133

Itoi, T., Mineta, S., Kimura, H., Yoshimi, K., Hirohashi, M., 2010. Fabrication and wear properties of Fe_3Al-based composites. Intermetalics 18, p. 2169.

Krein, R., Friak, M., Neugebauer, J., Palm, M., Heilmaier, M., 2010. L21-ordered Fe–Al–Ti alloys. Intermetallics 18, p. 1360.

Kumar M., Nautiyal T., Auluck S., 2009. First-principles calculations of electronic and optical properties of $Fe_{3-x}V_xAl$ (x = 0–3) compounds. Journal of Physics: Condensed Matter 44. p. 446001.

Lechermann F., Welsch F., Elsässer C., Ederer C., Fähnle M., Sanchez J., Meyer B., 2002. Density-functional study of Fe_3Al: LSDA versus GGA. Physical Review B 65, p. 3-6.

Maebashi T., Kozakai, T., Doi, M., 2004. Phase equilibria in iron-rich Fe-Al-V ternary alloy system. Zeitschrift für Metallkunde 95, p. 1005.

Methfessel M., Paxton A., 1989. High-precision sampling for Brillouin-zone integration in metals. Physical Review B 40, p. 3616

Morris D.G., Requejo L., Munoz-morris M., 2005. A study of precipitation in DO_3 ordered Fe–Al–Nb alloy. Intermetallics 13, p. 862-871.

Nishino Y., Kato M., Asano S., Soda K., Hayasaki M., Mizutani U., 1997. Semiconductor like Behavior of Electrical Resistivity in Heusler-type Fe_2VAl Compound. Physical Review Letters 79. p. 1909-1912.

Pack J., Monkhorst H., 1977. Special points for Brillouin-zone integrations'—a reply. Physical Review B 16, p. 1748

Palm M., 2009. Fe-Al materials for structural applications at high temperatures: Current research at MPIE, International journal of materials research 100, p. 277.

Palm, M., Krein, R., Milenkovic, S., Sauthoff, G., Risanti, D., Stallybrass, C., Schneider, A., 2007. Strengthening mechanisms for Fe-Al-based alloys with increased creep resistance at high temperatures. Materials Research Society Symposium Proceedings 980, p. 3.

Perdew J., Burke, K., Ernzerhof, M., 1996. Generalized Gradient Approximation Made Simple. Physical review letters 77, p. 3865

Prymak, O., Stein, F., 2010.Solidification and high-temperature phase equilibria in the Fe–Al-rich part of the Fe–Al–Nb system. Intermetallics 18, p. 1322.

Ramírez-Caballero G.E, Balbuena, P.B., Alonso, P.R., Gargano, P.H., Rubiolo, G.H., 2009. Carbon Adsorption and Absorption in the (111) $L1_2$ Fe_3Al Surface. The Journal of Physical Chemistry C 113, p. 18321

Schneider A., Zhang J., 2003. Metal dusting of ferritic Fe-Al-M-C (M = Ti, V, Nb, Ta) alloys in CO-H_2-H_2O gas mixtures at 650°C, Materials and Corrosion 54, p. 778

Schneider, A., Sauthoff, G., 2004. Iron aluminium alloys with strengthening carbides and intermetallic phases for high-temperature applications. Steel research international 75, p. 55.

Strauß, S., Krajak, R., Palm, M., Grabke, H.J., 1996. Metal dusting of Fe_3Al and $(Fe,Ni)_3Al$. Materials and Corrosion/Werkstoffe und Korrosion 47, p. 701

Taylor A., Jones R., 1958. Constitution and magnetic properties of iron-rich iron-aluminum alloys. Journal of Physics and Chemistry of Solids 6, p. 16-37.

Vanderbilt D., 1990. Soft self-consistent pseudopotentials in a generalized eigenvalue formalism. Physical Review B 41, p. 7892